Talanta 125 (2014) 36–44

Contents lists available at ScienceDirect

Talanta

journal homepage: www.elsevier.com/locate/talanta

Tetrabutylammonium-modified clay film electrodes: Characterization and application to the detection of metal ions

Adela Maghear [a,d,1], Mihaela Tertiş [a,b,1], Luminţa Fritea [a], Iuliu O. Marian [b], Emil Indrea [c], Alain Walcarius [d], Robert Săndulescu [a,*]

[a] Analytical Chemistry Department, Faculty of Pharmacy, "Iuliu Haţieganu" University of Medicine and Pharmacy, 4 Louis Pasteur Street, 400349 Cluj-Napoca, Romania
[b] "Babeş-Bolyai" University, Faculty of Chemistry and Chemical Engineering, 11 Arany Janos Street, 400028 Cluj-Napoca, Romania
[c] National Institute for R&D of Isotopic and Molecular Technologies, 65-103 Donath Street, 400295 Cluj-Napoca, Romania
[d] Laboratoire de Chimie Physique et Microbiologie pour l'Environnement, UMR 7564, CNRS – Université de Lorraine, 405 rue de Vandoeuvre, F-54600 Villers-lès-Nancy, France

ARTICLE INFO

Article history:
Received 7 October 2013
Received in revised form
17 February 2014
Accepted 19 February 2014
Available online 27 February 2014

Keywords:
Clay-modified electrode
Tetrabutylammonium
Permeability
Preconcentration electroanalysis
Metal ions
Square wave voltammetry

ABSTRACT

This work describes the preparation and characterization of smectite clay partially exchanged with tetrabutylammonium ions (TBA^+) and its subsequent deposition onto glassy carbon electrode (GCE) for application to the preconcentration electroanalysis of metal ions (Cd, Pb, and Cu). Such partial exchange of TBA^+ induces the expansion of the interlayer region between the clay sheets (as ascertained by XRD) while maintaining its ion exchange capacity, which resulted in enhanced mass transport rates (as pointed out by electrochemical monitoring of permeability properties of these thin (organo)clay films on GCE). This principle was applied here to the anodic stripping square wave voltammetric analysis of metal ions after accumulation at open circuit. Among others, detection limits as low as 3.6×10^{-8} M for copper and 7.2×10^{-8} M for cadmium have been achieved.

1. Introduction

Clay-modified electrodes (CLMEs) have been developed from few decades ago [1–3], but they still represent a notable field of interest, especially for their applications in electroanalysis, as discussed in some reviews [3–6] and illustrated in recent research papers where CLMEs have been used as sensors or biosensors (see examples, from our group [7–9] and from those of Ngameni [10–17], Mousty [18,19], or some others [20–22]). Clay minerals used as electrode modifiers are primarily (but not only) phyllosilicates-layered hydrous aluminosilicates. An important characteristic of those minerals is their interlayer distance which depends on the number of intercalated water and exchangeable cations within the interlayer space [4]. They also exhibit attractive properties such as a relatively large specific surface area, ion exchange capacity, and the ability to adsorb and intercalate some organic species. Smectites have been mostly used for CLMEs preparation in thin layer configuration, especially montmorillonite (MMT), due to a high cation exchange capacity (typically 0.80–1.50 mmol g^{-1}) and its thixotropy likely to generate stable and adhesive clay films on electrode surfaces [4,6].

Keeping in mind that clays are insulating materials, their use in electrochemistry thus requires a close contact to an electrode surface, which can be achieved via either the dispersion of clay powders in a conductive composite matrix (*e.g.*, carbon paste electrode [23]) or the deposition of clay particles as thin films on solid electrode surfaces. An advantage of the clay film modified electrodes is that they are binder-free, thanks to the particular platelet morphology of clay particles bringing them self-adhesive properties toward polar surfaces [5], which ensure a better interaction with most electrode materials and, consequently, a more durable immobilization. Clay films can be attached to a solid electrode surfaces by physical means (through solvent casting, spin-coating, or layer-by-layer assembly [5,6,24]), or electrophoretic deposition [25], by covalent bonding (via silane or alkoxysilane coupling agents) [26,27], or, more recently, in the form of clay–silica composite films [28]. At the beginning, CLMEs were mainly prepared from bare (unmodified) clay materials [5,6] but recent advances have been mainly based on organically-modified clays (obtained either by intercalation or grafting of organic moieties in the interlayer region of the clay [29–32]) because they enable to

* Corresponding author. Tel.: +40 264 582441, +40 745 770514.
E-mail address: rsandulescu@umfcluj.ro (R. Săndulescu).
[1] Equal contribution.

http://dx.doi.org/10.1016/j.talanta.2014.02.042
0039-9140

tune, control and extend the clay properties, resulting therefore to better analytical performance in terms of selectivity and sensitivity [10–17].

Dealing with sensitivity, preconcentration electroanalysis at modified electrodes (in which the analyte is firstly accumulated at open circuit and then electrochemically detected) has proven to be a powerful method to improve the performance of electrochemical sensors. In this respect, the ion exchange capacity of clays and the binding properties of organoclay have been exploited for the detection of metal ions using CLMEs (see examples in reviews [1,4]). Till now, however, very few examples are based on the use of intercalated organoclay materials for that purpose [11,16], in spite of the simpler modification procedure for intercalation than for grafting for instance (which requires the use of particular organoalkoxysilane reagents [10,15]). Here, we have thus examined the interest of CLMEs based on clay particles intercalated with tetrabutylammonium (TBA^+) moieties for the preconcentration electroanalysis of some metal ions (*i.e.*, Cd^{2+}, Pb^{2+} and Cu^{2+}). The choice of this tetraalkylammonium intercalation reagent was motivated by at least two features: (1) TBA^+ ions can be easily intercalated in the interlayer region of smectite clays by ion exchange [33], and (2) it modifies the packing configurations in the interlayer of the clay thus influencing the sorptive properties of the organoclay [34], notably with respect to adsorption of metal ions such as Cu^{2+} or Cd^{2+} [35,36].

The present study describes the deposition of partially TBA^+-modified clay particles (montmorillonite-rich natural clay from Romania) onto a glassy carbon electrode surface, subsequently covered with a dialysis tubing cellulose membrane, a configuration ensuring fast mass transport for analytes from the solution through the film to the electrode surface. The modified electrode was applied to the detection of some metal ions chosen as relevant biological and environmental contaminants (Cd^{2+}, Pb^{2+} and Cu^{2+}).

2. Experimental

2.1. Chemicals, reagents and clay materials

$NaNO_3$ (99%, Fluka), HCl (37%, Riedel de Haen), and tetrabutylammonium bromide (TBAB, 99%, Sigma) were used as received without further purification. The redox probes employed for permeability tests were of analytical grade: ferrocene dimethanol ($Fc(MeOH)_2$, Alfa Aesar); potassium hexacyanoferrate(III) ($K_3Fe(CN)_6$, Fluka); and hexaammineruthenium chloride ($Ru(NH_3)_6Cl_3$, Sigma-Aldrich). Single-component and multicomponent cation solutions were prepared daily by diluting standardized mother solutions (comprised of 1000 mg/l each metal ion, from Sigma-Aldrich). These standards were also used to certify copper(II) solutions prepared from $Cu(NO_3)_2 \cdot 3H_2O$ and 0.05 M HNO_3, lead (II) solutions prepared from $Pb(NO_3)_2$ and 0.5 M HNO_3 and cadmium(II) solutions prepared from $Cd(NO_3)_2 \cdot 4H_2O$ and 0.5 M HNO_3, Sigma-Aldrich, which were used to prepare diluted solutions for preconcentration studies (final pH in the electrolyte was 5.5 if not stated otherwise). The electrolyte employed was 0.1 M $NaNO_3$. All solutions were prepared with high purity water (18 MΩ cm^{-1}) from a Millipore milli-Q water purification system.

The clay sample used in this study was a natural Romanian clay from Valea Chioarului (Maramureş County), consisting mainly of MMT, with minor amounts of quartz. Its physico-chemical characterization is provided elsewhere [9]. The structural formula is $(Ca_{0.06}Na_{0.27}K_{0.02})_{\Sigma=0.35}$ $(Al_{1.43}Mg_{0.47}Fe_{0.10})_{\Sigma=2.00}$ $(Si_{3.90}Al_{0.10})_{\Sigma=4.00}$ $O_{10}(OH)_2 \cdot nH_2O$. It is characterized by a surface area (N_2, BET) of 190 $m^2\ g^{-1}$. Only the MMT-rich fine fraction of the clay (< 1 μm, as collected by sedimentation according to Stockes law, after the raw clay was suspended in water, ultrasonicated for about 15 min and allowed to settle, centrifugation and ultracentrifugation of the supernatant phase) was used here. This fine fraction has a cation exchange capacity (CEC) of 0.78 mequiv g^{-1} and was used before as template for an amperometric biosensor for acetaminophen detection [8]. Its XRD diffractogram showed a high content of MMT (with its characteristic peaks at 2θ: 6.94°; 19.96°; 21.82°; 28.63°; 36.14°; and 62,01°) and also confirmed the almost negligible presence of other minerals.

2.2. Apparatus and characterization procedures

Electrochemical experiments were carried out using a PGSTAT-12 potentiostat (EcoChemie) equipped with the GPES software. A conventional three electrode cell configuration was employed for the electrochemical measurements. Film modified GCEs were used as working electrodes, with an Ag/AgCl/KCl 3M reference electrode (Metrohm) and a platinum wire as reference and counter electrode. Cyclic voltammetry (CV) was carried out correspondingly in 1 mM $K_3Fe(CN)_6$, 0.1 mM $Ru(NH_3)_6Cl_3$, and 5 mM Fc $(MeOH)_2$ (in 0.1 M $NaNO_3$). CV curves were typically recorded in multisweep conditions at a potential scan rate of 20 mV s^{-1} and used to qualitatively characterize accumulation/rejection phenomena and mass transport issues through the various films.

Accumulation–detection experiments were also performed using copper(II), lead(II), and cadmium(II) as model analytes. Typically, open-circuit accumulation was made from diluted cations solutions (5×10^{-7}–10^{-6} M) at pH 5.5 and voltammetric detection was achieved after medium exchange to a cation-free electrolyte solution (0.1 M $NaNO_3$) by square wave voltammetry (SWV), at a scan rate of 5 mV s^{-1}, a pulse amplitude of 50 mV and a pulse frequency of 100 Hz.

The CNH elemental analysis of clay and organoclay materials was performed using an Elementar Vario Micro Cube, with the following experimental conditions: combustion temperature 950 °C; reduction temperature 550 °C; He flow 180 ml/min; O_2 flow 20 ml/min; and pressure 1290 mbar.

The film structure was characterized by X-ray diffraction (XRD), FTIR and Raman spectroscopy. XRD measurements were performed using a BRUKER D8 Advance X-ray diffractometer, with a goniometer equipped with a germanium monochromator in the incident beam, using Cu Kα1 radiation ($\lambda = 1.54056$ Å) in the 2θ range 15–85°. The FTIR spectra were measured on a Jasco FT/IR-4100 spectrophotometer equipped with Jasco Spectra Manager Version 2 software (550–4000 cm^{-1}). The Raman spectra were acquired with a confocal Raman microscope (Alpha 300R from WiTec) using a WiTec Control software for data interpretation (1000–3600 cm^{-1}, resolution > 0.5 cm^{-1}).

Electrochemical impedance spectroscopy (EIS) was used to characterize the electron transfer properties of the modified electrodes. The Nyquist plots were recorded with an Autolab potentiostat equiped with a FRA2 module and 4.9 version software.

2.3. Clay modification with TBAB

A MMT sample (10 g, particle size < 1 μm) was suspended in ultrapure demineralized water (clay concentration in water 4%). A quantity of Na_2CO_3 equivalent to 100 mequiv Na_2CO_3 per100 g clay was then added in the clay suspension and stirred for 30 min at 97 °C. An aqueous solution of TBAB (corresponding quantitatively to 1.1 times montmorillonite cation exchange capacity ($CEC_{MMT} = 0.78$ mequiv g^{-1}); 0.85 mequiv g^{-1} of TBAB), was then added and the suspension was stirred for 30 more minutes at room temperature. The obtained solid was separated by centrifugation and washed until it was free of any residual Br^-. The organoclay material was then dried for 48 h at 60 °C. When necessary, TBAB was partially solvent-extracted in an ethanol

solution containing 0.1 M $NaClO_4$ for 30 min under moderate stirring, to get partially TBA^+-exchanged clays.

2.4. Electrode assembly

Glassy carbon electrodes purchased from e-DAQ (GCEs, 1 mm in diameter) were first polished using 1 and 0.05 μm alumina powder and then washed with water and sonicated for 15 min in distilled water to remove any alumina trace, leading to an electrochemically active surface area of 7.85×10^{-3} cm^2. Clay or organoclay suspensions (5 mg/ml) were prepared in distilled water (20 min stirring+10 min sonication), and left quiescent at room temperature.

The clay or organoclay film was deposited on GCE by spin-coating. A volume of 2.5 μl of the clay suspension (5 mg/ml) was deposited on the electrode surface and then stirred for 20 min at 2000 rotation per minute. The electrode was then dried at room temperature for 1 h. The clay or organoclay film was covered with a dialysis tubing cellulose membrane (Sigma) fixed first with a rubber o-ring, and then with laboratory film to avoid the solution penetration under the membrane.

The five systems characterized in this study are: the bare glassy carbon electrode (GCE), the bare glassy carbon electrode with cellulose membrane (GCE/M), the unmodified MMT film coated on GCE with cellulose membrane (GCE+MMT/M), and the TBAB modified MMT film coated on GCE with cellulose membrane before (GCE+MMT+TBAB/M) and after partial TBA^+ extraction (GCE+MMT+$TBAB_{(partial)}$/M).

3. Results and discussions

3.1. Characterization of clay materials and clay film electrodes

3.1.1. Physico-chemical characterization of (organo)clays

XRD was first used to characterize the structural changes of the smectite clay, which are likely to occur upon intercalation of TBAB. As expected, prior to surfactant entrapment, the clay film exhibited the same MMT characteristics as those reported for the raw clay particles in Section 2 (diffraction lines at 2θ values (deg) of 6.9; 19.9; 21.8; 28.6; 36.1; 62.0, and data not shown). As the clay was in contact with a TBAB solution, the unit cell parameters and the profile discrepancy indices values (Table 1) indicate an expansion of the interlayer region between the clay sheets. This expansion is due to the incorporation of TBA^+ species in the clay interlayer (in agreement with a similar process described elsewhere for other surfactants such as cetyltrimethylammonium bromide [37]). After partial removal of TBA^+, in the conditions described in Section 2, the clay interlayer distance was found to maintain almost the same values obtained for the fully doped clay, MMT+TBAB (Table 1). The partial TBA^+ removal was otherwise confirmed by CHN elemental analysis (Table 2), showing that about 1/3 of the initially exchanged TBA^+ remained in the material after ethanol/$NaClO_4$ treatment.

Table 1
Unit cell parameters and profile (R_p) discrepancy indices calculated by Rietveld refinement analysis of XRD data for the pristine clay (MMT), the clay exchanged with TBAB (MMT+TBAB) and clay with TBAB after partial TBA^+ removal (MMT+$TBAB_{(partial)}$).

Samples	a [Å]	b [Å]	c [Å]	R_p
MMT	5.17	5.17	12.62	17.2
MMT+TBAB	5.24	5.24	15.49	18.6
MMT+$TBAB_{(partial)}$	5.23	5.23	15.48	17.6

Table 2
Elemental analysis of the modified clay before and after TBA^+ partial extraction.

Samples	N (%)	C (%)	H (%)
MMT+TBAB	0.73	8.82	4.07
MMT+$TBAB_{(partial)}$	0.26	3.85	3.39

The modified clays were also characterized by vibrational spectroscopy (Fig. S1), in order to support its reaction with TBAB and partial removal of TBA^+.

The main information of FTIR data is that the typical bands of TBAB can be found in addition to the clay ones in both MMT+TBAB and MMT+$TBAB_{(partial)}$ samples (confirming successful incorporation of TBA^+), but with less intense TBA^+ signals in the latter case (confirming the effectiveness of the partial removal process). In more detail, the FTIR spectrum of Valea Chioarului clay (Fig. S1A, black line) presents the typical bands attributed to the characteristic groups of MMT, as described elsewhere [8,38]. The FTIR spectrum of TBAB (Fig. S1A, blue line) presents at 739 cm^{-1} a band corresponding to the C–H alkanes rocking vibration. The band near 1020–1250 cm^{-1} can be assigned to the C–N stretching vibrations and the bands near 1450–1470 cm^{-1} are due to the C–H alkanes bending vibrations. The bands near 1350–1370 cm^{-1} correspond to the C–H alkanes rocking vibrations and the bands near 2969–2945 cm^{-1} to the C–H alkanes stretching vibrations. The bands near 600–1300 cm^{-1} can be assigned to the C–C aliphatic chain vibrations [39]. For the clay sample fully doped with TBAB (Fig. S1A, red line), the bands at 3625 cm^{-1} (stretching vibration of the hydroxyl group), near 1637 cm^{-1} (bending vibration of H–O–H group) and in the 1000–1200 cm^{-1} region (Si–O stretching vibration) are common with MMT spectrum [8,38]. In addition, one can see the bands near 2969–2945 cm^{-1} (C–H alkanes stretching), near 1475 cm^{-1} (C–H alkanes bending), and near 1350 cm^{-1} (C–H alkanes rocking), all indicating the presence of TBA^+ in the clay. It can be assumed that the broad band at 1000–1200 cm^{-1} includes the C–N stretching vibrations [8,38,39]. After partial removal of the modifier, the FTIR spectrum (Fig. S1A, green line) presents almost the bands that were attributed to TBA^+, yet with much lower intensities.

Similar conclusions can be drawn from Raman spectra. In detail, the Raman spectrum of MMT is characterized by three strong bands near 200, 425 and 700 cm^{-1}, (Fig. S1B, black line) [40–42]. The sharp Raman peak at 706 cm^{-1} is due to SiO_4 vibrations and the broader feature near 420 cm^{-1} that has been assigned to M–OH bending vibrations [40,42] and to Si–O–Si(Al) bending modes [41,42]. The position of the strong band near 201 cm^{-1} varies depending on the clay mineral type [40,42]; it is probably due to the SiO_4 and influenced by Al substitution and the dioctahedral or trioctahedral character. Weaker bands due to the OH bending vibration are observed near 850–920 cm^{-1} [42]. In the case of TBAB spectra (Fig. S1B, blue line), the sharp Raman bands near 2800–3000 cm^{-1} are due to the C–H bending vibrations. The strong bands near 250–400 cm^{-1} can be assigned to the C–C aliphatic chains vibrations. The broader feature near 1380 cm^{-1} can be assigned to the CH_3 bending vibration, while the feature near 1460 cm^{-1} is due to the asymmetric CH_3 vibrations. The band near 1331 cm^{-1} corresponds to the C–N bending vibration and the weaker band near 1057 cm^{-1} is due to the C–C aliphatic chain vibrations [43]. The Raman spectra of the TBA^+ modified MMT exhibit, as expected from elemental analysis data (Table 2), both characteristic bands of MMT and TBAB, yet with lower intensity for the organic component in MMT+$TBAB_{(partial)}$ (Fig. S1B, green line) than in MMT+TBAB (Fig. S1B, red line).

From all these results (XRD, FTIR, Raman and elemental analysis), one can conclude that successful incorporation of TBA^+

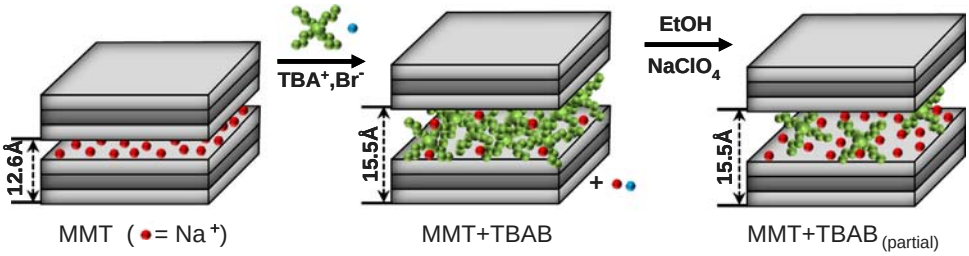

Scheme 1. Illustration of the modification of MMT with TBAB and partial removal of TBA^+.

in the clay was achieved, resulting in an increase in the interlayer distance between the clay sheets, this latter being maintained expanded after moderate (*i.e.*, 2/3) removal of the organic modifier (see illustration in Scheme 1).

3.1.2. Permeability properties of clay film electrodes

Multisweep cyclic voltammetry was applied to evaluate the permeability properties of the clay and organoclay film electrodes, firstly using a cationic redox probe ($Ru(NH_3)^{3+}$), and the main results are shown in Fig. 2. Comparing the response on the bare GCE (Fig. 1A) and the same electrode covered with the cellulose membrane (Fig. 1B) shows that this dialysis membrane acts somewhat as a physical barrier, restricting mass transport rates, as peak current values were ca. 2 times lower than on the bare electrode. Nevertheless this membrane was necessary to maintain good mechanical stability of the clay films. In the presence of the pristine MMT clay, the physical barrier was even more pronounced in the first CV scans but the signals then rapidly and continuously increased upon successive potential cycling (Fig. 1C) to reach a plateau at 3.1 μA after ca. 25 cycles. This value is 2.7 times larger than peak currents recorded at the bare GCE (1.15 μA). Such behavior is classically observed at clay films electrodes [44] and it is evidently due to the accumulation of $Ru(NH_3)^{3+}$ species by ion exchange with sodium ions in the clay film. Effective accumulation thus occurred in spite of the presence of the cellulose overlayer membrane. The accumulation behavior was also observed using the organoclay films but it exhibited distinct features (Fig. 1D and E). For the fully doped MMT+TBAB material (Fig. 1D), the maximal current values were restricted to about 2/3 of the MMT film value (Fig. 1C), consistent with lower ion exchange capacity values reported for TBAB-modified clays with respect to the pristine ones [35,36]. More interesting is the behavior of the $MMT+TBAB_{(partial)}$ film (Fig. 1E) exhibiting not only larger steady-state peak currents than the MMT clay film but also significantly faster accumulation rates (compare curves *E* and *C* in Fig. 1F). This attractive feature can be explained by the much easier and faster access to the ion exchange sites thanks to the expansion of the interlayer region between the clay sheets by TBAB while maintaining a high exchange capacity as a result of only partial exchange of sodium ions with TBA^+. These results suggest promising use of $GCE+MMT+TBAB_{(partial)}/M$ for preconcentration electroanalysis of cationic analytes (see Section 3.2. for confirmation).

When using an anionic probe ($[Fe(CN)_6]^{3-}$) or a neutral one ($Fc(MeOH)_2$), the situation was totally different, the negatively-charged probe being totally excluded from the clay film (Fig. 2A) due to electrostatic repulsion, while poor accumulation of the neutral probe was observed (Fig. 2B), the (organo)clay layer acting only as a physical barrier.

3.1.3. EIS characterization

EIS was employed to characterize the electron transfer properties of the modified electrodes. The typical Nyquist plot of EIS includes a semicircle and a liniar zone, which correspond to the electron transfer limited process and the diffusion limited process, respectively. The proposed circuit is R1(Q1[R2W1]) both for unmodified GCE and GCE modified with MMT (with or withoutTBAB). The conventional C_{dl} is replaced by the constant phase element (CPE), representing the non-uniform behavior of adsorbed species on irregular geometry and small electrode surface. The reaction seems to occur in single step and a combination of kinetic and diffusion processes with infinite thickness describe the whole process. The high frequency section of Nyquist curves describe an arc (Fig. 3), the diameter of which displays the R_{ct} values (namely the electron transfer resistance), that increases in the presence of MMT from 128 Ω (GCE) to 395 Ω ($GCE+MMT+TBAB_{(partial)}/M$), indicating better electrode surface coverage with non-conductive clay film in the latter case. The experimental results of EIS confirmed that the clay films coated well the GCE surface and the clay's presence decreases the electron transfer rate of the redox probe.

3.2. Preconcentration electroanalysis of metal ions – effect of experimental conditions

The organoclay film electrodes have been examined for metal ions detection (mainly Cu^{2+} and Cd^{2+}, but also Pb^{2+}) via preconcentration electroanalysis, involving two successive steps: an open-circuit accumulation by ion exchange, followed by anodic stripping voltammetry detection (in the SWV mode) after medium exchange.

3.2.1. Influence of the supporting electrolyte on the detection step

Due to the insulating character of the organoclay material, the quantitative electrochemical detection of the accumulated metal ions requires their beforehand complete desorption and concomitant electroreduction onto the electrode surface prior to anodic stripping. It is thus necessary to select the most appropriate supporting electrolyte likely to fulfill these requirements. Various media (such as 0.1 M HCl, 0.2 M HNO_3, 0.1 M KCl, and 0.1 M $NaNO_3$) have been tested after 5 min accumulation at open-circuit from 10^{-5} M Cu^{2+} solution using $GCE+MMT+TBAB_{(partial)}/M$ system. It appears that the DWV response was of the same order of magnitude in all cases (data not shown), yet slightly lower (by ca. 20%) in chloride media. Among the best media (HNO_3 and $NaNO_3$), 0.1 M $NaNO_3$ was chosen as the most appropriate supporting electrolyte as it gave rise to a sharper stripping signal and better long-term stability (acidic solutions are good desorption media but they also contribute to the chemical degradation of the clay via hydrolysis of the aluminum sites [45]). In addition, the electrolysis time to be applied before anodic stripping detection should be long enough to ensure complete reduction of all the accumulated Cu(II) species, and 3 min was found to be a suitable value. The $NaNO_3$ medium and 3 min electrolysis time were thus used in all further detection experiments.

3.2.2. Effect of the accumulation time

The effect of accumulation time was studied in a range from 0 to 25 min and typical results are presented in Fig. 4 for Cu^{2+} at 3 distinct concentrations. For larger concentrations (see parts (b) and (c) in Fig. 4), the current response first increased with the accumulation

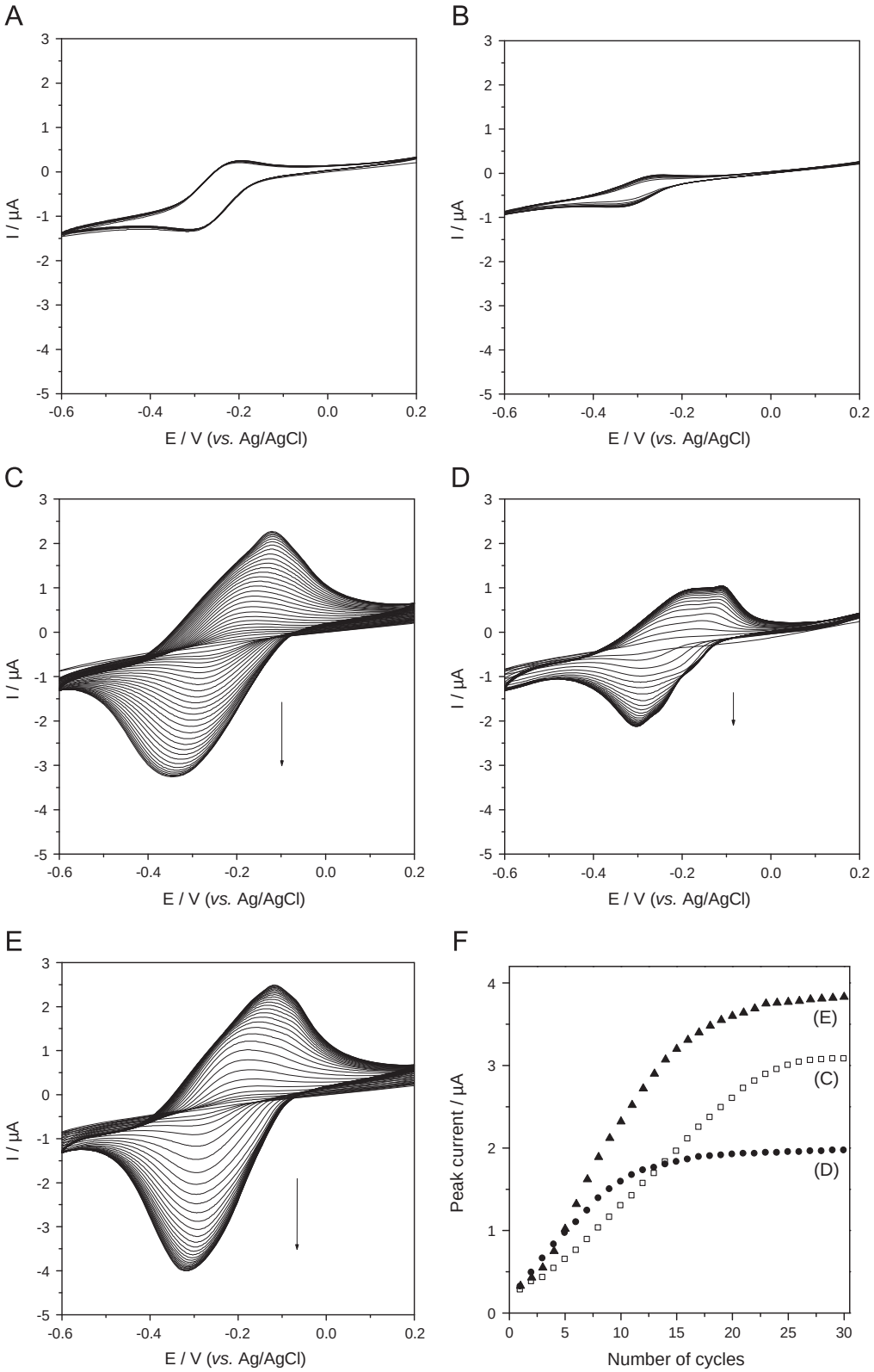

Fig. 1. (A–E) Multisweep cyclic voltammograms recorded in 10^{-3} M $Ru(NH_3)_6Cl_3$ (in 0.1 M $NaNO_3$) using: (A) bare GCE (10 cycles); (B) GCE/M (10 cycles); (C) GCE+MMT/M (30 cycles); (D) GCE+MMT+TBAB/M (30 cycles); (E) and GCE+MMT+$TBAB_{(partial)}$/M (30 cycles). (F) Variation in peak currents as a function of the number of cycles for cases (C)–(E).

time and then tended to level off and reached almost steady-state after more than 15 min. This can be attributed to the saturation of the accessible adsorption sites in the clay film, as typical for preconcentration electroanalysis at modified electrodes [46–49]. At lower concentration (see part (a) in Fig. 4), a period is required to sufficiently accumulate the metal ions at detectable levels, after which the electrode response was linear with the accumulation time. Such trend was previously observed with other modified electrodes. Accordingly, the preconcentration time should be appropriately set with respect to the analyte concentration in the accumulation medium.

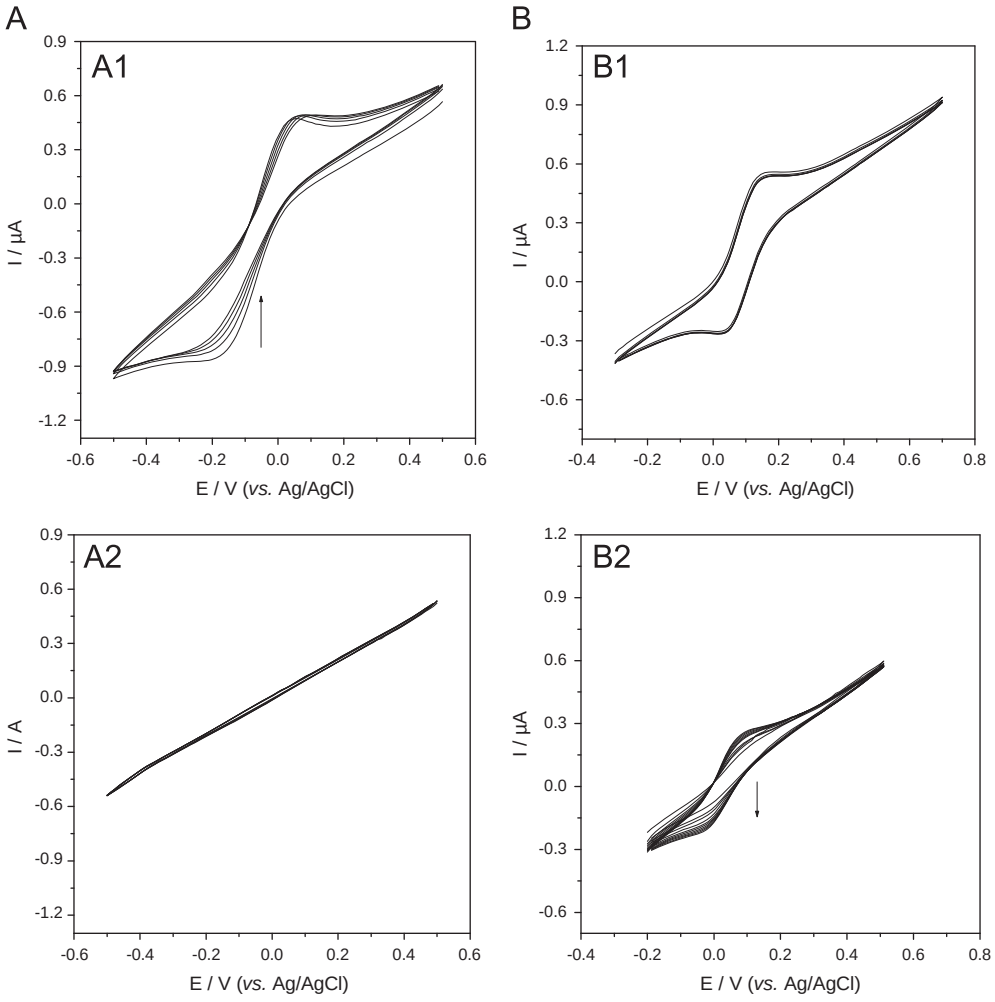

Fig. 2. Multisweep CVs recorded in (A) 10^{-3} M $[Fe(CN)_6]^{3-}$ or (B) 10^{-3} M $Fc(MeOH)_2$ (in 0.1 M $NaNO_3$) using (A1 and B1) GCE/M or (A2 and B2) GCE+MMT+$TBAB_{(partial)}$/M.

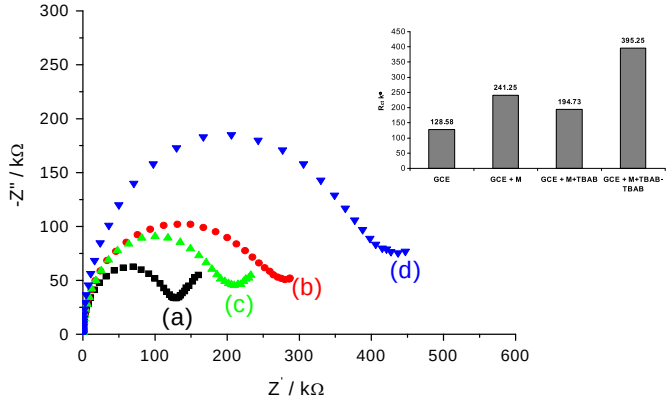

Fig. 3. Nyquist plots for GCE/M (a), GCE+MMT/M (b), GC+MMT+TBAB/M (c), and GC+MMT+$TBAB_{(partial)}$/M (d), obtained in 10 mM $K_3[Fe(CN)_6]$ in PBS (0.1 M; pH 7.4). Inset: R_{ct} variation with the electrode type (EIS conditions: amplitude 0.005; frequency range: 100 kHz to 0.01 Hz; number of frequencies: 71).

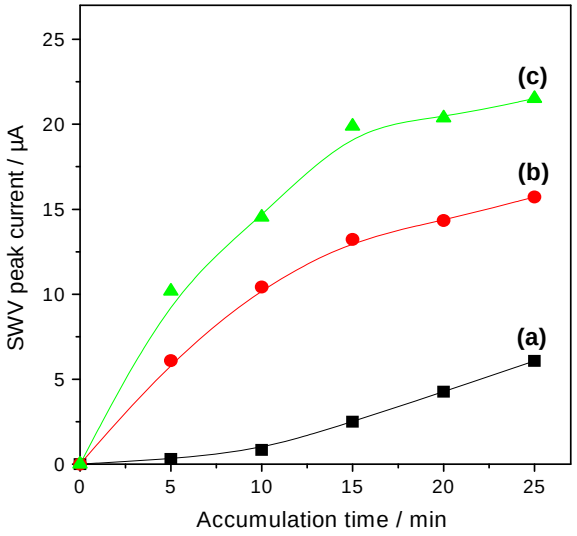

Fig. 4. Variation of peak currents with accumulation time after open circuit accumulation of Cu(II) at 3 distinct concentrations at GCE+MMT+$TBAB_{(partial)}$/M: (a) 5×10^{-7} M, (b) 10^{-6} M, and (c) 5×10^{-6} M. Detection was performed in 0.1 M $NaNO_3$.

3.2.3. *Effect of the presence of TBA^+ in the clay*

The effect of TBA^+ insertion in the clay interlayer on the (organo)clay film electrode response was studied both for Cu^{2+} and Cd^{2+} analysis after 5 min accumulation at open-circuit. From Fig. S2A and B one can observe that the response obtained with GCE+MMT+$TBAB_{(partial)}$/M was larger by about two times with respect to GCE covered with the pristine MMT clay film. This result is consistent with the permeability data discussed above (see Section 3.1.2), for which faster mass transport was observed with the MMT+$TBAB_{(partial)}$ film (Fig. 1F), thanks to the presence of some TBA^+ species in the interlayer region of the clay contributing to expand the interlayer distance between the clay sheets while

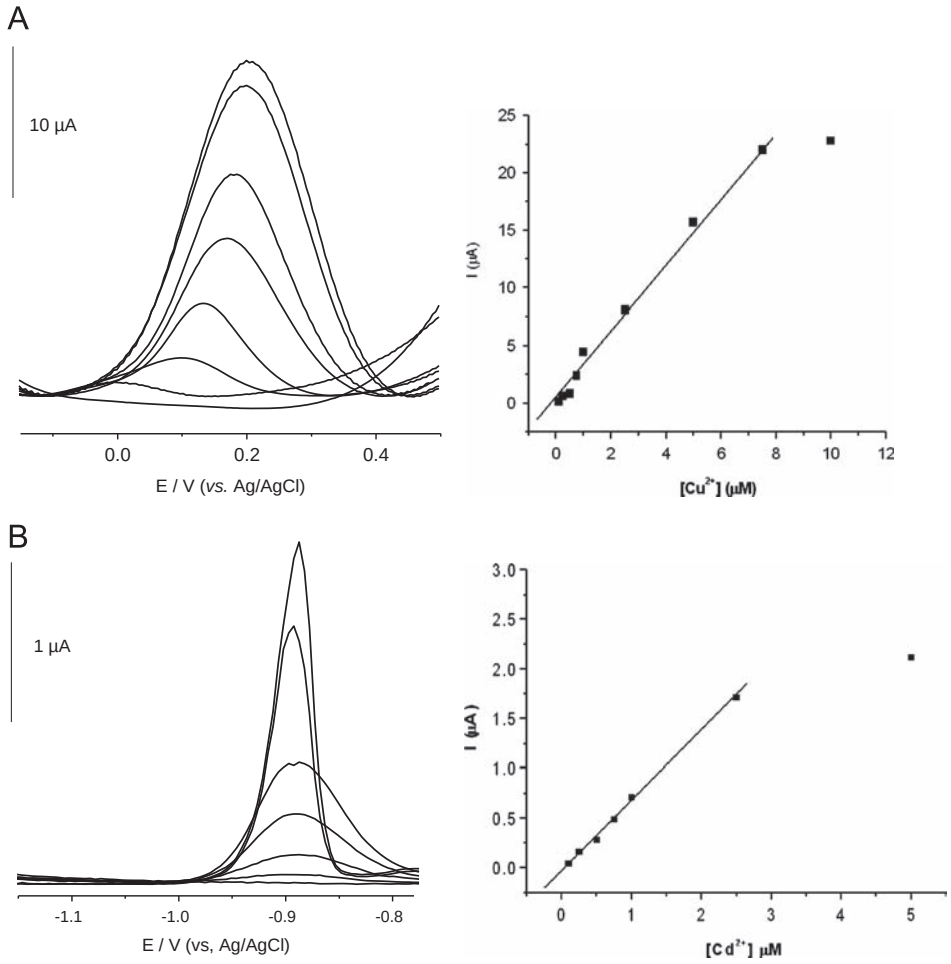

Fig. 5. Calibration data obtained with GCE+MMT+$TBAB_{(partial)}$/M for the analysis of Cu^{2+} (A) and Cd^{2+} (B) (conditions as in Fig. 4). The insets show some corresponding calibration plots.

maintaining its ion exchange capacity (Scheme 1). As the rate determining step of preconcentration electroanalysis is the diffusion of the analyte to the binding sites in the material, the sensitivity of the process is therefore enhanced in conditions of improved mass transport. GCE+MMT+$TBAB_{(partial)}$/M was thus exclusively used afterwards for analytical purposes.

3.2.4. Regeneration, reproducibility and operational stability

It can be also seen from Fig. S3 that the GCE+MMT+$TBAB_{(partial)}$/M electrode can be easily regenerated by back ion exchange, just via soaking some time (typically 2 min) in the electrolyte solution. Following this preconcentration/detection/regeneration scheme, 10 consecutive voltammetric measurements were performed using the same modified electrode in order to determine the system's stability towards Cu^{2+} and Cd^{2+} analysis. The GCE+MMT+$TBAB_{(partial)}$/M electrode exhibited good long-term operational stability for both Cu^{2+} (Fig. S3A) and Cd^{2+} (Fig. S3B) and good reproducibility (the relative standard deviations were 0.35% and 1.55%, respectively for Cu^{2+} and Cd^{2+}). This good performance can be ascribed to the durable immobilization of the clay material (by the aid of the cellulose membrane) and the effectiveness of both the accumulation and regeneration steps thanks to fast mass transport processes ensured by the porous electrode modifier.

3.2.5. Calibration data

The calibration curves obtained for Cu^{2+} and Cd^{2+} at GCE+MMT+$TBAB_{(partial)}$/M are shown in Fig. 5. There were no noticeable anodic peaks when the experiments were performed in Cu^{2+}- and Cd^{2+}-free solutions. In the case of copper (Fig. 5A), the peak was quite large and centered around +0.2 V (*vs.* Ag/AgCl), yet undergoing some cathodic shift at lower Cu^{2+} concentrations, whereas the detection of cadmium (Fig. 5B) led to sharper anodic peaks located at −0.9 V (*vs.* Ag/AgCl) independently on the Cd^{2+} concentration. Both analytes gave rise to rather similar calibration curves, starting with a linear variation which tended to level off afterwards. The relationship between Cu^{2+} concentration and current intensity obtained with SWV was linear in a range from 1.2×10^{-7} M to 7.5×10^{-6} M, according to the equation I (μA)= 2.98 ± 0.11 [Cu^{2+}] (μM)+0.23 ± 0.04 with a correlation coefficient of 0.9922 (8 points considered for the linear plot). In the case of Cd^{2+}, the linear range extended from 2.16×10^{-7} M to 2.5×10^{-6} M, according to the equation I (μA)=$0.70\pm0.01\cdot$[Cd^{2+}] (μM)+ 0.028 ± 0.017 with a correlation coefficient of 0.9983 (6 points considered for the linear plot). The LOD values were estimated on the basis of a signal-to-noise ratio of 3 [15], while the LOQ values were estimated on the basis of a signal-to-noise ratio of 10. For copper, the LOD was estimated at 3.6×10^{-8} M and LOQ=1.09×10^{-7} M, whereas cadmium analysis gave rise to a LOD of 7.2×10^{-8} M and LOQ=2.16×10^{-7} M.

3.2.6. Simultaneous analysis of multi-component cationic solutions

Fig. S4 compares the voltammetric response of a multi-component solution of Cd^{2+}, Pb^{2+} and Cu^{2+} (10^{-5} M each), recorded using GCE+MMT+$TBAB_{(partial)}$/M, to the signals

Table 3
Interference study for analysis of 1 μM Cu^{2+} or Cd^{2+} at GCE+MMT+$TBAB_{(partial)}$/M.

Interfering ion	Analyte signal (%)	
	Cu^{2+}	Cd^{2+}
Cu^{2+}	–	98.9
Cd^{2+}	99.6	–
Co^{2+}	100.0	99.5
Pb^{2+}	101.2	99.8
Ni^{2+}	84.4	88.6
Zn^{2+}	97.3	93.2
Ba^{+}	99.4	99.1
Na^{+}	98.9	99.3
K^{+}	100.5	99.1

obtained for the corresponding mono-component solutions analyzed in the same conditions. One can see that the interactions between the three cations is minimal in terms of peak current intensity variations, but the cadmium peak is slightly shifted to less potentials, and that of copper to less anodic values, whereas the position of the lead peak was almost unaffected by the presence of the other metal ions. This suggests possible analysis of these metal ions in mixture.

3.2.7. *Interference study*

The selectivity of the GCE+MMT+$TBAB_{(partial)}$/M-based sensor for Cu^{2+} and Cd^{2+} was evaluated in the presence of some common metal ions expected to influence its response (*i.e.*, Pb^{2+}, Co^{2+}, Ni^{2+}, Zn^{2+}, Ba^{+}, Na^{+}, and K^{+}, tested at the same concentration as the target analytes: 10^{-6} M Cu^{2+} and Cd^{2+}). The recovery data are given in Table 3. Most of these species do not influence the electrochemical signal of Cu^{2+} and Cd^{2+} in a significant way, except Ni^{2+} for which a noticeable decrease (12–16%) in intensity was observed.

4. Conclusions

This work demonstrates that low-cost pillared clay is an attractive material likely to be used as electrode modifier for the elaboration of electrochemical sensors. The effective functionalization of MMT by ion exchange with tetrabutylammonium bromide was first confirmed by XRD, FT-IR and Raman spectroscopies, and EIS determinations. Then, the electrochemical characterization of permeability properties of thin films of organoclay on GCE revealed that the functionalized material kept its ion exchange properties after partial TBA^{+} removal and exhibited excellent permeability issues and long-term mechanical stability. The permeability properties of such thin organoclay films towards selected redox probes were characterized, pointing out the crucial interest to use partially TBA^{+}-exchanged clays to ensure effective accumulation rates of positively-charged species. These advantageous features can be notably exploited in preconcentration electroanalysis, with improved sensitivities in comparison to similar electrodes covered with the unmodified clay film. In spite of the fact that the sensor assembly seems complicated, the possibility to reuse the same sensor it is an advantage, because it can be easily regenerated in a very simple manner and short time, without losing the initial performances. The organoclay film electrode offers the advantage of ease of fabrication and exhibits good analytical performance in terms of linear response range and good repeatability for the accumulation/detection of metal ions such as Cu^{2+}, Cd^{2+}, or Pb^{2+}. After optimization of various experimental parameters, a stable and reliable sensor was obtained. This low-cost device could be of interest in environmental monitoring of these toxic pollutants.

Acknowledgments

We thank the INCDTIM Cluj-Napoca, for providing access to crystallographic facilities and for recording XRD spectra. We also acknowledge Tamara Topală for FTIR imaging (UMF Iuliu Haţieganu Cluj-Napoca), Gabriel Katona (Universitatea Babeş-Bolyai Cluj-Napoca) for the elemental analysis, Mircea Puia (Universitatea Babeş-Bolyai Cluj-Napoca) and Adrian Pîrnău (INCDTIM Cluj-Napoca) for Raman spectra recording and interpretation. The authors are grateful to the Agence Universitaire de la Francophonie, to POS-DRU 88/1.5/S/58965, and PNII IDEI Grant no. 338/2011 for financial support.

Appendix A. Supplementary material

Supplementary data associated with this article can be found in the online version at http://dx.doi.org/10.1016/j.talanta.2014.02.042.

References

[1] A. Fitch, Clays Clay Miner. 38 (1990) 391–400.
[2] S.M. Macha, A. Fitch, Microchim. Acta 128 (1998) 1–18.
[3] J.-M. Zen, A.S. Kumar, Anal. Chem. 76 (2004) 205A–211A.
[4] Z. Navrátilová, P. Kula, Electroanalysis 15 (2003) 837–846.
[5] C. Mousty, Appl. Clay Sci. 27 (2004) 159–177.
[6] C. Mousty, Anal. Bioanal. Chem. 396 (2010) 315–325.
[7] A. Maghear, A. Cernat, C. Cristea, A. Marian, I.O.Marian, R. Săndulescu, New electrochemical sensors based on clay and carbon micro and nanoparticles for pharmaceutical and environmental analysis, in: Technical Proceedings of the 2012 NSTI Nanotechnology Conference and Expo, NSTI-Nanotech 2012, June 18–21, 2012, Santa Clara, CA, vol. 1, 2012, pp. 574–577.
[8] A. Maghear, C. Cristea, A. Marian, I.O. Marian, R. Săndulescu, Farmacia 61 (2013) 1–11.
[9] A. Maghear, C. Cristea, A. Marian, I.O. Marian, R. Săndulescu, Farmacia 61 (2013) 648–657.
[10] I.K. Tonlé, E. Ngameni, A. Walcarius, Sens. Actuat. B B110 (2005) 195–203.
[11] E. Ngameni, I.K. Tonlé, J.T. Apohkeng, R.G.B. Bouwé, A. Jieumboué-Tchinda, A. Walcarius, Electroanalysis 18 (2006) 2243–2250.
[12] J. Kemmegne-Mbouguen, E. Ngameni, A. Walcarius, Anal. Chim. Acta 578 (2006) 145–155.
[13] A. Jieumboué-Tchinda, E. Ngameni, A. Walcarius, Sens. Actuat. B B121 (2007) 113–123.
[14] I.K. Tonlé, E. Ngameni, H.L. Tcheumi, V. Tchieda, C. Carteret, A. Walcarius, Talanta 74 (2008) 489–497.
[15] I.K. Tonlé, S. Letaief, E. Ngameni, C. Detellier, Electroanalysis 23 (2011) 245–252.
[16] R.G.B. Bouwé, I.K. Tonlé, S. Letaief, E. Ngameni, C. Detellier, Appl. Clay Sci. 52 (2011) 258–265.
[17] J. Kemmegne-Mbouguen, I.K. Tonlé, A. Walcarius, E. Ngameni, Talanta 85 (2011) 754–762.
[18] K. Charradi, C. Forano, V. Prévot, A. Ben Haj Amara, C. Mousty, Langmuir 25 (2009) 10376–10383.
[19] F. Charmantray, N. Touisni, L. Hecquet, C. Mousty, Electroanalysis 25 (2013) 630–635.
[20] N.L. Dias Filho, D. Ribeiro do Carmo, Talanta 68 (2006) 919–927.
[21] H. Chen, Z. Zhang, D. Cai, S. Zhang, B. Zhang, J. Tang, Z. Wu, Anal. Sci. 27 (2011) 613–616.
[22] B. Demir, M. Seleci, D. Ag, S. Cevik, E.E. Yalcinkaya, D.O. Demirkol, U. Anik, S. Timur, RSC Adv. 3 (2013) 7513–7519.
[23] I. Svancara, K. Kalcher, A. Walcarius, K. Vytras, Electroanalysis With Carbon Paste Electrodes, Analytical Chemistry Series, CRC Press, Taylor and Francis Group, Boca Raton, FL, USA, 2012.
[24] C.-H. Zhou, Z.-F. Shen, L.-H. Liu, S.-M. Liu, J. Mater. Chem. 21 (2011) 15132–15153.
[25] C. Song, G. Villemure, J. Electroanal. Chem. 462 (1999) 143–149.
[26] D. Rong, Y.I. Kim, T.E. Mallouk, Inorg. Chem. 29 (1990) 1531–1535.
[27] L. Coche-Guérente, S. Cosnier, V. Desprez, P. Labbé, D. Petridis, J. Electroanal. Chem. 401 (1996) 253–256.
[28] A. Maghear, M. Etienne, M. Tertiş, R. Sandulescu, A. Walcarius, Electrochim. Acta 112 (2013) 333–341.
[29] K.A. Carrado, Appl. Clay Sci. 17 (2000) 1–23.
[30] F. Wypych, Interface Sci. Technol. 1 (2004) 1–56.

[31] M. Jaber, J. Miehe-Brendle, in: V. Valtchev, S. Mintova, M. Tsapatsis (Eds.), Ordered Porous Solids: Recent Advances and Prospects, Elsevier, Stevenson Ranch, 2009, pp. 31–39 (Chapter 2).
[32] H. He, Q. Tao, J. Zhu, P. Yuan, W. Shen, S. Yang, Appl. Clay Sci. 71 (2013) 15–20.
[33] M. Akcay, J. Colloid Interface Sci. 296 (2006) 16–21.
[34] Y. Chun, G. Sheng, S.A. Boyd, Clays Clay Miner. 51 (2003) 415–420.
[35] K.G. Bhattacharyya, S. Sen Gupta, Sep. Purif. Technol. 50 (2006) 388–397.
[36] S. Sen Gupta, K.G. Bhattacharyya, J. Hazard. Mater. 128 (2006) 247–257.
[37] W. Xue, H. He, J. Zhu, P. Yuan, Spectrochim. Acta A 67 (2007) 1030–1036.
[38] A. Marian, I.O. Marian, C. Cristea, R. Săndulescu, G. Vasilie, Study of Some Clay Minerals Used in Electrode Making With Application in Environment Chemistry, Studia UBB, Ambientum, LIV (2009) 67–75.
[39] G. Socrates, Infrared and Raman Characteristic Group Frequencies: Tables and Charts, John Wiley and Sons (2001) 277–278.
[40] E. Loh, J. Phys. C: Solid State Phys. 6 (1973) 1091–1104.
[41] R.L. Frost, L. Rintoul, Appl. Clay Sci. 11 (1996) 171–183.
[42] J.L. Bishop, E.J. Murad, Raman Spectrosc. 35 (2004) 480–486.
[43] ⟨http://www.horiba.com/fileadmin/uploads/Scientific/Documents/Raman/bands.pdf⟩.
[44] I.K. Tonlé, E. Ngameni, A. Walcarius, Electrochim. Acta 49 (2004) 3435–3443.
[45] N.T. Coleman, Econ. Geol. 57 (1962) 1207–1218.
[46] A. Walcarius, T. Barbaise, J. Bessière, Anal. Chim. Acta 340 (1997) 61–76.
[47] S. Sayen, C. Gérardin, L. Rodehuser, A. Walcarius, Electroanalysis 15 (2003) 422–430.
[48] S. Goubert-Renaudin, M. Etienne, Y. Rousselin, F. Denat, B. Lebeau, A. Walcarius, Electroanalysis 21 (2009) 280–289.
[49] V. Marchal, F. Barbier, F. Plassard, R. Faure, O. Vittori, Fresenius J. Anal. Chem. 363 (1999) 710–712.